Astronomy & Astrophysics manuscript no. crab_paper
February 19, 2018

Crab nebula polarization observations at 150 GHz with NIKA

A. Ritacco[1,8⋆], J.F. Macías-Pérez[1], N. Ponthieu[10], R. Adam[1,2], P. Ade[5], P. André[4], A. Beelen[6], A. Benoît[7], A. Bideaud[7], N. Billot[8], O. Bourrion[1], A. Bracco[4], M. Calvo[7], A. Catalano[1], G. Coiffard[3], B. Comis[1], A. D'Addabbo[7,9], F.-X. Désert[10], S. Doyle[5], J. Goupy[7], C. Kramer[8], G. Lagache[11], S. Leclercq[3], J.-F. Lestrade[17], P. Mauskopf[5,12], F. Mayet[1], A. Maury[4], A. Monfardini[7], F. Pajot[6], E. Pascale[5], L. Perotto[1], G. Pisano[5], M. Rebolo-Iglesias[1], V. Revéret[4], L. Rodriguez[4], C. Romero[3], H. Roussel[16], F. Ruppin[1], K. Schuster[3], A. Sievers[8], C. Thum[8], S. Triqueneaux[7], C. Tucker[5], and R. Zylka[3]

[1] Laboratoire de Physique Subatomique et de Cosmologie, Université Grenoble Alpes, CNRS/IN2P3, 53, avenue des Martyrs, Grenoble, France
[2] Laboratoire Lagrange, Université Côte d'Azur, Observatoire de la Côte d'Azur, CNRS, Blvd de l'Observatoire, CS 34229, 06304 Nice cedex 4, France
[3] Institut de RadioAstronomie Millimétrique (IRAM), Grenoble, France
[4] Laboratoire AIM, CEA/IRFU, CNRS/INSU, Université Paris Diderot, CEA-Saclay, 91191 Gif-Sur-Yvette, France
[5] Astronomy Instrumentation Group, University of Cardiff, UK
[6] Institut d'Astrophysique Spatiale (IAS), CNRS and Université Paris Sud, Orsay, France
[7] Institut Néel, CNRS and Université Grenoble Alpes, France
[8] Institut de RadioAstronomie Millimétrique (IRAM), Granada, Spain
[9] Dipartimento di Fisica, Sapienza Università di Roma, Piazzale Aldo Moro 5, I-00185 Roma, Italy
[10] Univ. Grenoble Alpes, CNRS, IPAG, F-38000 Grenoble, France
[11] Aix Marseille Université, CNRS, LAM (Laboratoire d'Astrophysique de Marseille) UMR 7326, 13388, Marseille, France
[12] School of Earth and Space Exploration and Department of Physics, Arizona State University, Tempe, AZ 85287
[13] Université de Toulouse, UPS-OMP, Institut de Recherche en Astrophysique et Planétologie (IRAP), Toulouse, France
[14] CNRS, IRAP, 9 Av. colonel Roche, BP 44346, F-31028 Toulouse cedex 4, France
[15] University College London, Department of Physics and Astronomy, Gower Street, London WC1E 6BT, UK
[16] Institut d'Astrophysique de Paris, Sorbonne Universités, UPMC Univ. Paris 06, CNRS UMR 7095, 75014 Paris, France
[17] LERMA, CNRS, Observatoire de Paris, 61 avenue de l'Observatoire, Paris, France

Received February 19, 2018 / Accepted –

ABSTRACT

The Crab nebula is a supernova remnant exhibiting a highly polarized synchrotron radiation at radio and millimeter wavelengths. It is the brightest source in the microwave sky with an extension of few arcminutes and commonly used as standard candle for any experiment which aims at measuring the polarization of the sky. Though its spectral energy distribution has been well characterized in temperature, in polarization the amount of data is still mediocre. We report in this paper high resolution (18″ FWHM) observations of the Crab nebula in total intensity and linear polarization at 150 GHz with the *NIKA* camera. *NIKA*, operated at the IRAM 30 m telescope from 2012 to 2015, is a camera made of Lumped Element Kinetic Inductance Detectors (LEKIDs) observing the sky at 150 and 260 GHz. From these observations we are able to reconstruct the spatial distribution of the Crab nebula polarization degree and angle, which is found to be compatible with previous observations at lower and higher frequencies. Averaging across the source and using other existing data sets we find that the Crab nebula polarization angle is consistent with being constant over a wide range of frequencies with a value of $-87.9° \pm 0.3$ in Galactic coordinates. We also present the first estimation of the Crab nebula Spectral Energy Distribution polarized flux in a wide frequency range: 30-350 GHz. Using the data set available so far we have estimated the polarization spectral index β_{pol}=-0.35 ± 0.03.

Key words. Techniques: Crab nebula – Tau A – polarization – KIDs – individual: NIKA

1. Introduction

The Crab nebula (or Tau A) is a plerion-type supernova remnant emitting a highly polarized signal (Weiler & Panagia 1978; Michel et al. 1991). Referring to Hester (2008), from inside out the Crab consists of a pulsar, the synchrotron nebula, a bright expanding shell of thermal gas, and a larger very faint freely expanding supernova remnant.

Near the center of the nebula a shock is observed as formed by the jet thermalized and pulsar's ultra-relativistic wind which is confined by the thermal ejecta from the explosion (Weisskopf et al. 2000; Wiesemeyer et al. 2011). The synchrotron emission from the nebula is observed in the radio frequency domain as powered by the pulsar located at equatorial coordinates (J2000) $R.A. = 5^h34^m31.9383014^s$ and $Dec. = 22°0'52.17577''$ (Lobanov et al. 2011) through its jet.

The polarization of the Crab nebula radio emission, discovered in 1957 independently by Mayer et al. (1957) and Kuz'min & Udal'Tsov (1959) has confirmed that the synchrotron emission as the underlying mechanism.

⋆ Corresponding author: Alessia Ritacco, ritaccoa@iram.es

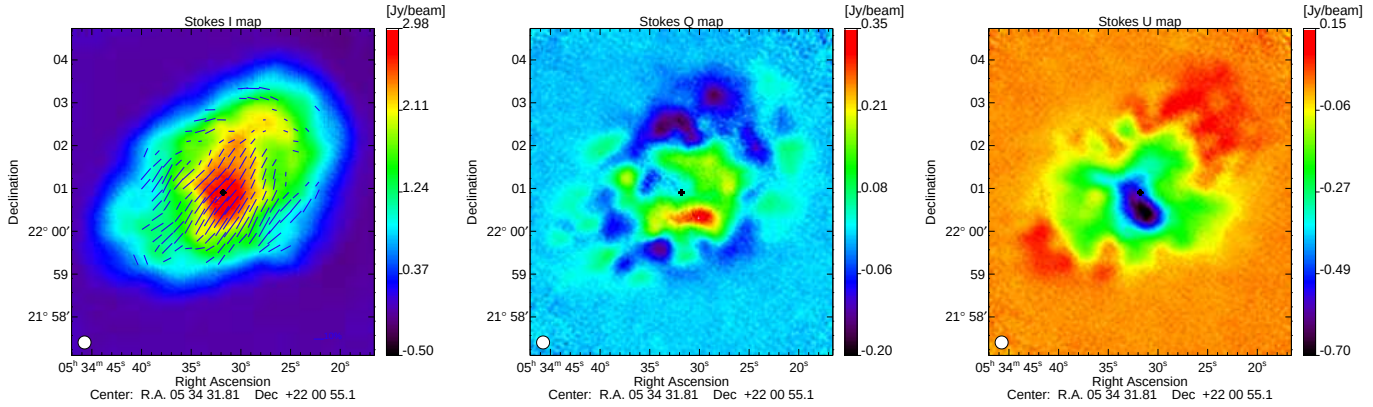

Fig. 1. From left to right: Crab nebula Stokes I, Q and, U maps shown here in Equatorial coordinates obtained at 150 GHz with the *NIKA* camera. Polarization vectors, indicating both the polarization degree and the orientation, are over-plotted in white on the intensity map where the polarization intensity satisfies $I_{pol} > 3\sigma_{I_{pol}}$ and $I_{pol} > 0.1$ Jy. The *NIKA* FWHM is shown in the lower left. The black cross marks the pulsar position.

Today the Crab nebula is perhaps the most observed object in the sky beyond our own solar system and often used as calibrator by new instruments. It is also quite isolated with low background diffuse emission.

In particular it is the most intense polarized astrophysical object in the microwave sky at angular scales of few arcminutes and for this reason it is chosen not only for high resolution cameras but also for the calibration of CMB polarization experiments, which have beamwidths comparable to the extension of the source. Indeed, upcoming CMB experiments aiming at measuring the primordial $B-$modes require an accurate determination of the foreground emissions to the CMB signal and a high control of systematic effects. The Crab nebula has already been used for polarization cross-check analysis in the frequency range from 30 to 353 GHz (Weiland et al. 2011; Planck Collaboration et al. 2016).

High angular resolution observations from the XPOL experiment (Thum et al. 2008) at the IRAM 30 m telescope have revealed the spatial distribution of the Crab Nebula in intensity and polarization at 90 GHz with an absolute accuracy of 0.5° in the polarization angle (Aumont et al. 2010). This observation has also showed that the polarization spatial distribution varies from the source peak to the edges of the source and evidences the need of an accurate study at high resolution in a large frequency range to be able to use this source as a calibrator for future polarization esperiments.

Previous studies (Macías-Pérez et al. 2010) of the total Spectral Energy Distribution (SED) of the Crab nebula have shown a spectrum well described by a single synchrotron component at radio and mm wavelengths and predict negligible variations in polarization fraction and angle in the frequency range of interest for CMB studies.

Observations of the polarization of the Crab Nebula have been performed with the *NIKA* camera (Monfardini et al. 2010; Catalano et al. 2014; Monfardini et al. 2014) at the IRAM 30 m telescope during the observational campaign of February, 2015. A first overview of the *NIKA* Crab polarization observations, focusing on instrumental characterization of the polarization system, was given in Ritacco et al. (2016). In this paper we go a step further in the analysis by combining *NIKA* observations with published values at other frequencies to trace the polarized SED of the Crab nebula. We use polarization observations from the *WMAP* satellite at 23, 33, 41, 61 and 94 GHz (Weiland et al. 2011), from the *Planck* satellite at 30, 44, 70, 100, 143, 217, 353 GHz and from XPOL/30m at 90 GHz (Aumont et al. 2010).

The paper is organized as follows: in Sec. 2 the intensity and polarization maps obtained with the *NIKA* camera are presented together with the polarization degree and angle spatial distributions; Sec. 3 presents the reconstruction of the polarization properties of the Crab nebula in well defined regions; Sec. 4 presents the Crab nebula SED in temperature and polarization; in Sec. 5 we present our conclusions.

2. *NIKA* observations of the Crab Nebula

2.1. NIKA camera and polarization setup

NIKA is a dual band camera observing the sky in intensity and polarization at 150 and 260 GHz with 18 arcsec and 12 arcsec FWHM resolution, respectively. It has a Field-of-View (FoV) of 1.8′ at both wavelengths. It was operated at the IRAM 30 m telescope between 2012 and 2015. A detailed description of the *NIKA* camera can be found in Monfardini et al. (2010, 2011) and Catalano et al. (2014).

In addition to total power observations, *NIKA* was also a test bench for the polarization system of the final instrument *NIKA2* (Calvo et al. 2016; Catalano et al. 2016; Adam et al. 2017), which was installed at the telescope in October, 2015. The polarization setup of *NIKA* and consists in a continuously rotating metal mesh half wave plate (HWP) followed by an analyzer, both at room temperature and placed in front of the entrance window of the cryostat. The *NIKA* Lumped Elements Kinetic Inductance Detectors (LEKIDs) are not intrinsically sensitive to polarization. The HWP rotates at 2.98 Hz that modulates the polarization signal at 4×2.98 Hz. With a typical telescope scanning speed of 26.23 arcsec/s. This provides a quasi-simultaneous measure of Stokes parameters I, Q and U per beam and places the polarized power in the frequency domain far from the low frequency electronic noise and the atmospheric fluctuations. Ritacco, A. et al. (2017) gives more details on the *NIKA* polarization capabilities and describes the performance of the instrument at the telescope. In particular the sensitivity of the *NIKA* camera in polarization mode was estimated to be 50 mJy.$s^{1/2}$ at 150 GHz.

NIKA has provided the first polarization observations performed with Kinetic Inductance Detectors, confirming that KIDs are a suitable detector technology for the development of the next generation of polarization sensitive experiments.

2.2. NIKA observations

Crab nebula polarization observations with the *NIKA* camera were performed at the IRAM 30 m telescope in February, 2015. The average effective opacity at 150 GHz was $\tau = 0.2$. Fig. 1 shows the Stokes I, Q and U maps obtained by a co-addition of 14 maps of 8×6 arcminutes for a total observation time of $\sim$ 2.4 hours. The maps were performed in equatorial coordinates in four different scan directions: 0°, 90°, 120°, 150°. This allowed us to have the best coverage of the source.

To obtain the Stokes I, Q, and U Crab nebula maps in Equatorial coordinates, we have used a dedicated polarization data reduction pipeline (Ritacco, A. et al. 2017), which is an extension of the total intensity *NIKA* pipeline (Catalano et al. 2014; Adam et al. 2014). The main steps of the polarization pipeline are summarized below:

1. Subtraction of the HWP induced parasitic signal, which is modulated at harmonics of the HWP rotation frequency and represents the most tedious noise contributing to the polarized signal.
2. Reconstruction of the Stokes I, Q and U time ordered information (TOI) from the raw modulated data. This is achieved using a demodulation procedure consisting in a lock-in around the fourth harmonic of the HWP rotation frequency, where the polarization signal is located.
3. Subtraction of the atmospheric emission in the demodulated TOIs using decorrelation algorithms. In polarization, the HWP modulation reduces significantly the atmospheric contamination and there is no need to further decorrelate the Q and U TOI's from residual atmosphere. By contrast, in intensity the atmospheric emission fully dominates the signal and to recover the large angular scales we use the 260 GHz band as an atmosphere dominated band like in Adam et al. (2014). This decorrelation impacts the reconstructed Stokes maps via a transfer function, see Fig. 2. We have estimated this function with simulated observations of diffuse emission that were passed through the data reduction pipeline, with the exact same scanning, sample flagging and data processing as real data. We found that the power spectrum of the output maps match that of the input one to better than 1% (resp. 5%) on scales smaller (resp. larger) than $\sim 1'$. The impact of the data processing is thus negligible compared to uncertainties on absolute calibration on small scales, and its moderate effect on large angular scales is further reduced with the subtraction of a zero level for the photometry (see below). In the following, we therefore neglect this transfer function.
4. Correction of the intensity-to-polarization-leakage-effect, which was identified in observations of unpolarized sources like the planet Uranus. For point sources the effect was about 3% peak-to-peak, while for extended sources like the Crab nebula it has been found to be the order of 0.5 % peak-to-peak. Ritacco, A. et al. (2017) describes the algorithm of leakage correction developed specifically for *NIKA* polarization observations. Applying this algorithm to Uranus observations the instrumental polarization is reduced to 0.6% of the total intensity I.
5. Projection of the demodulated and decorrelated Stokes I, Q, and U TOIs into Stokes I, Q and U equatorial coordinates maps.

2.3. Crab polarization properties

In this section we discuss the polarization properties of the source in terms of polarization degree p and angle ψ, which are

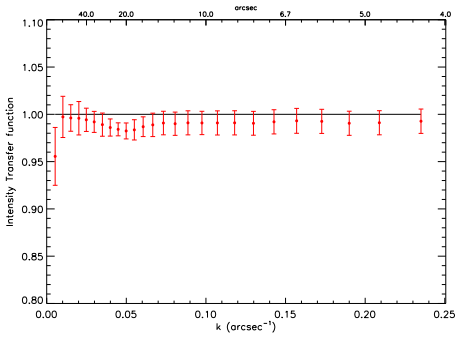

Fig. 2. Top: Transfer function of the data processing in temperature.

defined through the Stokes parameters I, Q, and U as follows:

$$p = \frac{\sqrt{Q^2 + U^2}}{I}$$

and

$$\psi = \frac{1}{2} \arctan \frac{U}{Q}. \quad (1)$$

These definitions are not linear in I, Q and U and therefore, the observational uncertainties have to be carefully considered, *i.e.* p, ψ are noise biased. Simmons et al. (1980); Simmons & Stewart (1985); Montier et al. (2015) proposed analytical solutions to correct for this bias. For intermediate and high S/N ratio the polarization degree and its uncertainty read:

$$\begin{aligned} p &= \frac{\sqrt{Q^2 + U^2 - \sigma_Q^2 - \sigma_U^2}}{I}, \\ \sigma_p &= \frac{\sqrt{Q^2\sigma_Q^2 + U^2\sigma_U^2 + p^4 I^2 \sigma_I^2}}{pI^2}. \end{aligned} \quad (2)$$

Furthermore, the polarization angle in a high S/N regime can be approximated by Eq. 1 with the uncertainty

$$\sigma_\psi = \frac{\sqrt{Q^2\sigma_Q^2 + U^2\sigma_U^2}}{2(pI)^2}. \quad (3)$$

The spatial distribution map of the polarization degree p of the Crab nebula without noise bias correction is presented on the top left panel of Fig. 3.

The polarization degree p reaches a value of 20.9 ±0.8 % at the peak of the total intensity, which is consistent with what observed on the top right panel of Fig. 3, where the variation of p as a function of the Stokes I is shown. Here the p values have been noise bias corrected and satisfy the condition $I_{pol} = \sqrt{Q^2 + U^2} > 5\,\sigma_{I_{pol}}$. The distribution of the polarization degree appears highly dispersed around a mean value of 20%. The compatibility between the p value computed at the Stokes I peak position and the above mentioned plot is expected because we use a very high S/N ratio threshold of $5\,\sigma_{I_{pol}}$, which restricts the measurement to a small region around the peak of the source. In addition, the p value found is also consistent within the error bars with POLKA experiment measurement (Wiesemeyer et al. 2014) (cf. Table 1).

The polarization degree decreases towards the edges of the source. Furthermore, the high polarization degree observed at the extremities of the source is misleading and caused by the very low S/N ratio of the Stokes I map observed in these regions.

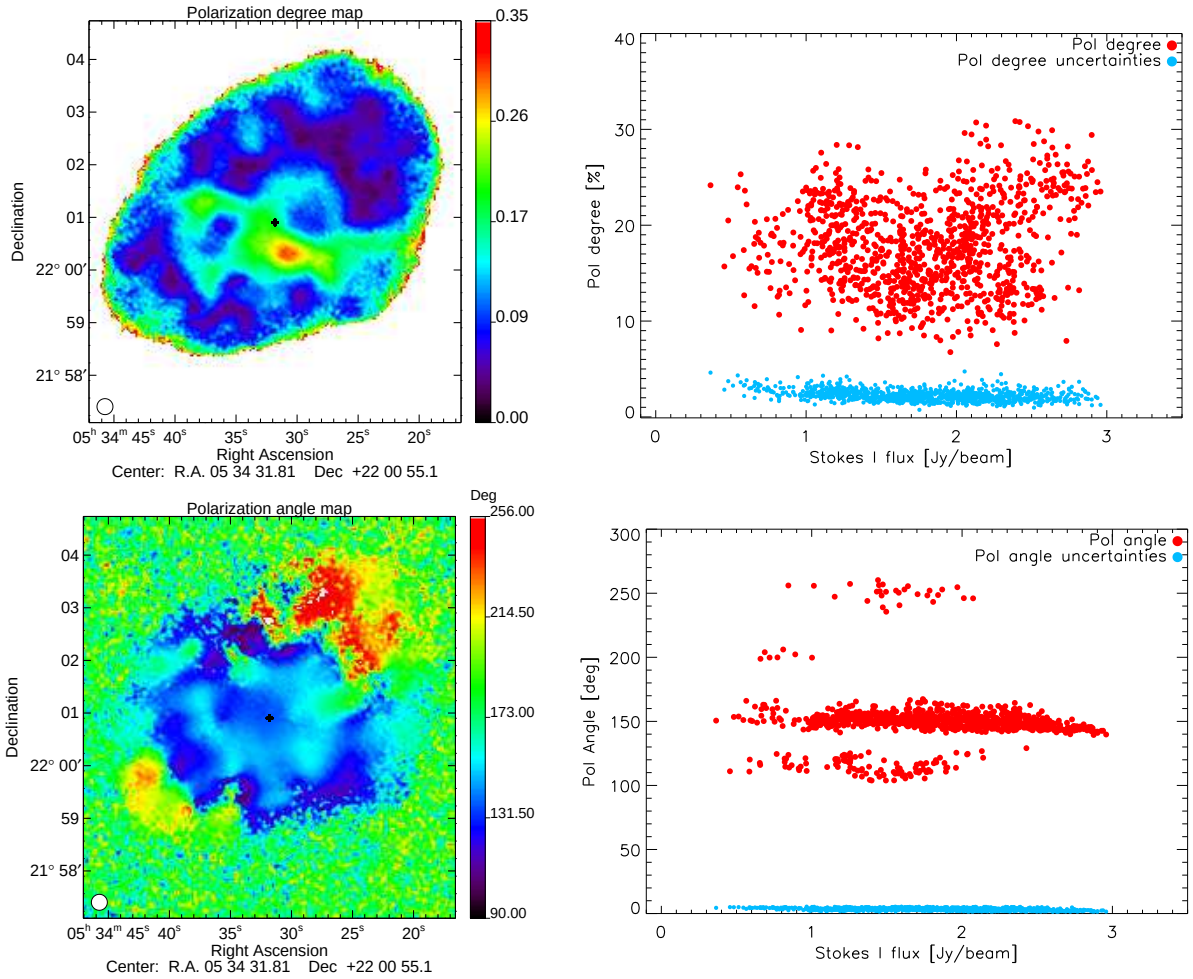

Fig. 3. *Top*: The left panel shows the polarization degree map p, uncorrected for noise bias, of the Crab nebula. The right panel shows the noise bias corrected p values as a function of total intensity map (Stokes I). The condition $I_{pol} > 5\sigma_{I_{pol}}$ is satisfied for those values. *Bottom*: on the left we present the polarization angle map ψ (Equatorial coordinates system) of the Crab nebula. On the right panel the distribution of ψ values is represented as a function of the total intensity in the case of very high S/N ratio where $I_{pol} > 5\sigma_{I_{pol}}$. The cyan dots represent the uncertainties calculated as the dispersion between different observational scans. The black cross marks the pulsar position on the maps.

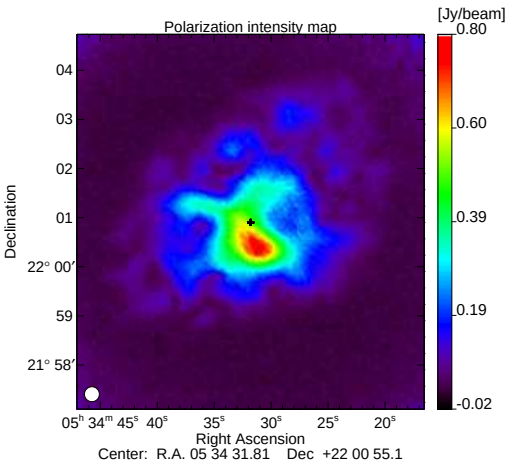

Fig. 4. *NIKA* polarized intensity map of the Crab nebula at 150 GHz. The map shows high polarized emission reaching a value of 0.8 Jy beam^{-1}. The telescope beam FWHM is shown in the lower left. The black cross marks the pulsar position.

The variation of p highlights the interest of high resolution polarization observations of the Crab nebula.

The bottom left panel of Fig. 3 shows the spatial distribution of polarization angle ψ. We observe a relatively constant polarization angle of about 150 ° represented here in equatorial coordinates, except for the northern region where the averaged angle is around 220°, and some inner regions with lower polarization angle. These values are confirmed by the bottom right panel that shows the polarization angle distribution as a function of total intensity satisfying the condition $I_{pol} > 5\sigma_{I_{pol}}$.

The sudden change of polarization angle on the northern region was already observed by the XPOL experiment at 90 GHz (Aumont et al. 2010). This together with the variation of the polarization fraction discussed above confirms the need of high angular resolution observations at low and high frequencies for a good understanding of the Crab polarized emission properties. High resolution observations give the possibility to estimate the polarization properties at different scales and compare with low resolution experiments, like CMB experiments.

We present in Fig. 4 the 150 GHz Crab polarization intensity map I_{pol} uncorrected for noise bias. We observe a peak at 0.8 Jy beam^{-1} and the polarization decreases towards the edges of the nebula.

	I [Jy]	p [%]	ψ [°]
		Pulsar	
POLKA	1.63	25.3 ± 3.0	145.1 ± 3.3
XPOL		13.9 ± 0.6	158.1 ± 0.5
SCUPOL		14.3 ± 1.8	140.0 ± 2.8
NIKA	8.4 ± 0.1	18.1 ± 0.8	138.5(-80.9) ± 0.1 ± 1.8
		Peak	
POLKA	1.72	25.0 ± 3.1	151.7 ± 3.5
XPOL		25	149.0 ± 1.4
SCUPOL		18.7 ± 1.5	146.1 ± 2.1
NIKA	8.3 ± 0.1	20.9 ± 0.8	140.2(-82.6) ± 0.04 ± 1.8

Table 1. Values estimated by POLKA (870 μm), XPOL (3 mm), SCUPOL (850 μm) reported in Wiesemeyer et al. (2014) and *NIKA* (this paper) at the pulsar and peak position, respectively. For *NIKA* the position of the pulsar, represented on the maps by a black cross, refers to Lobanov et al. (2011). The position of the peak of the total intensity has equatorial coordinates (J2000) $R.A. = 5^h34^m32.380422^s$ and $Dec. = 22°0'44.098276''$. The polarization angle is given in Equatorial coordinates and in Galactic coordinates within parenthesis. A systematic angle uncertainty of 1.8° must be considered. A total calibration error of 10 % must be accounted for and propagated to the polarization estimates.

2.4. Comparison to other high resolution experiments

In this section we compare *NIKA* results at the pulsar position and Stokes I map peak with high angular resolution experiments such as POLKA, XPOL and SCUPOL. These observe at wavelengths of 870 μm, 3 mm and 850 μm, respectively. Tab. 1 reports the measurement of the polarization properties, degree and angle, performed by these experiments (Wiesemeyer et al. 2014). The values show a significant discrepancy in terms of polarization angle estimated at the pulsar position. Though POLKA and SCUPOL agree at 1σ level, XPOL show a much higher angle. At the position of the Stokes I peak the three experiments are consistent between each other. Generally, the values estimated with *NIKA* are consistent within 3σ level with POLKA and SCUPOL experiments, but they disagree the XPOL values, which show higher values in both positions.

3. Total intensity and polarization fluxes

We compute the total flux across the Crab nebula, which has an extent of about 5′x7′ as shown in Fig. 1. We use standard aperture photometry techniques to calculate the flux as shown in Fig. 5. We use as center position the center of the map with equatorial coordinates (J2000) $R.A. = 5^h34^m31.95^s$ and $Dec. = 22°0'52.1''$. A zero level in the map, calculated as the mean of the signal measured on an external annular ring region (see bottom panel of Fig. 5) of radius $4' < R < 4.5'$, has been subtracted from the map. The total signal estimated is 204.4±7.9±10.2 Jy. The first uncertainty term accounts for statistical uncertainties computed from fluctuations of the signal at large radii. We use Uranus for absolute point source flux calibration. The flux of the planet is estimated from a frequency dependent model of the planet brightness temperature as described in Moreno (2010). This model is integrated over the *NIKA* bandpasses for each channel, and it is assumed to be accurate at the 5% level. The final absolute calibration factor is obtained by fitting the amplitude of a Gaussian function of fixed angular size on the reconstructed maps of Uranus, which represents the main beam. For the polarization observational campaign of February 2015 this uncertainty is estimated to be 5% for the *NIKA* 2.05 mm channel (150 GHz) (Ritacco, A. et al. 2017). Nevertheless, as described in Adam et al. (2014); Catalano et al. (2014), by integrating the Uranus flux up to 100 arcsec, we observe that the total solid angle covered by the beam is larger than the Gaussian best-fit of the main beam by a factor of 28%. As consequence we account for this factor in the estimation of the fluxes. Moreover, Adam et al. (2014) estimated the uncertainty on the solid angle of the main beam to be 4%. Finally, the overall calibration error is estimated to be about 10%, by considering also the uncertainties on the side lobes.

The polarization efficiency factor estimated across the *NIKA* 2.05 mm spectral band and reported in Ritacco, A. et al. (2017) is $\rho_{pol} = 0.9941 \pm 0.0002$. This very small efficiency lost of 0.6 % has a very small impact on the estimation of the polarization fluxes and the calibration error itself.

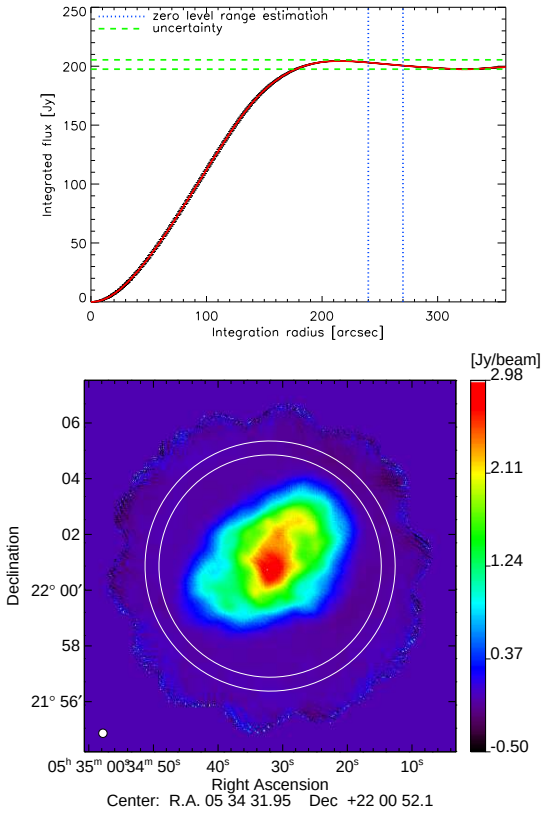

Fig. 5. Top: Cumulative flux of the Crab nebula (top) obtained at 150 GHz over 4′ from the center obtained by aperture photometry. The flux has been corrected by a zero level in the map, which corresponds to the mean of the signal calculated in an annular ring as indicated by the white circles on the map (bottom) and by the blue dotted lines on the top. The green dotted line represents the uncertainties measured at large radii.

In order to compare our results with low angular resolution CMB experiments, we present in Tab. 2 the polarization degree p and angle ψ integrated values obtained in well defined regions: 5′, 7′ FWHM from the center of the maps.

The polarization angles are here presented in Equatorial coordinates and Galactic coordinates, within parenthesis, to ease the comparison with the *Planck* (Planck Collaboration et al. 2016) and *WMAP* CMB experiments (Weiland et al. 2011). As discussed in Ritacco, A. et al. (2017) a 1.8° uncertainty must be considered because the mechanical motor, in which the HWP is mounted, completes 100 steps per tour of the HWP. Therefore, it

is the precision associated to the determination of the HWP zero, corresponding to its optical axis in the cabin reference frame.

As stated in 2.3, we use simple Gaussian estimators in this work that are unbiased only at high S/N ratio. This adds an additional uncertainty on the determination of the degree of polarization p and on the angle ψ when the SNR is not larger than $\sim 3\sigma$. While we can delimit regions of the map as a function of their SNR to give reliable results per pixel, the determination of average quantities over the entire map is more delicate. **Taking the entire map and averaging it over Gaussian beams of 5′ and 7′ FWHM, we find $\psi = -82.4 \pm 0.2^\circ \pm 1.8^\circ$ and $\psi = -83.3 \pm 0.3^\circ \pm 1.8^\circ$ respectively, while we find $-87.6 \pm 0.1^\circ \pm 1.8^\circ$ if we consider only pixels with a I_{pol} SNR larger than 3 in both regions. Morevover we also consider an uncertainty of 0.5° due to leakage effect subtraction, which is estimated from the comparison of the maps before and after leakage correction. The angle averaged in the Gaussian beams are more affected by the noise on the maps but still consistent with the case of high S/N. In terms of polarization degree, we find $p = 8.2 \pm 0.1\%$ and $p = 6.9 \pm 0.1$ if we take all the pixels to average Q and U over our fiducial beams of 5′ and 7′, respectively. The statistical uncertainty accounts for montecarlo simulation of the noise in Q and U, the angle estimation difference between two sets of jack-knife maps, 7 maps each.**

Fig. 6 shows the polarization fraction (top) and polarization angle (bottom) of the Crab nebula as a function of the frequency as measured by five different instruments: *Planck* (Planck Collaboration et al. 2016), *WMAP* (Weiland et al. 2011), XPOL (Aumont et al. 2010) and *NIKA* (this paper). Notice that the *Planck* satellite FWHMs are: 33′, 24′, 14′, 10′, 7.1′, 5.5′, 5′ arcminutes at 30, 44, 70, 100, 143, 217, 353 GHz, respectively. *WMAP* satellite has FWHMs: 0.93°, 0.68°, 0.53°, 0.35°, <0.23° at 22 GHz, 30 GHz, 40 GHz, 60 GHz, 90 GHz respectively.

The solid line in both figures represents the weighted-average found using all the observations shown and the dashed lines represent the uncertainties estimated on the weighted-average. Considering only low frequency data (<200 GHz) and excluding the XPOL data (see below) we find that the degree of polarization of the Crab nebula at arcmin scales is 6.95±0.03 %. In terms of degree of polarization most data sets are consistent at the 2σ level with the weighted-average value. For XPOL the discrepancy can probably be explained by the lower sensitivity of the single channel XPOL experiment to the lower than average polarization of the outer parts of the nebula. POLKA show a very high polarization degree due to the ∼40% flux loss observed in Stokes I, see Fig. 7. This is compatible with the losses expected due to the spatial filtering in LABOCA data reduction in this range of angular scales (Belloche et al. 2011). In the case of *Planck* most of the results are consistent with average value.

The weighted-average of the polarization angle of the Crab nebula at ≥ 5′ scales is therefore estimated considering all available observations, is -87.9° ± 0.3.

All the observations shown on the bottom panel of Fig. 6 agree within 1σ with this value except for *NIKA* and POLKA. For *NIKA* and POLKA we have used a FWHM of 7 arcmin to estimate the polarization angle and degree values represented in the plot of Fig. 6. We find a very good agreement between these two high angular resolution experiments and *NIKA* is also consistent within 1σ with *Planck* value at 143 GHz and 2σ with the average value.

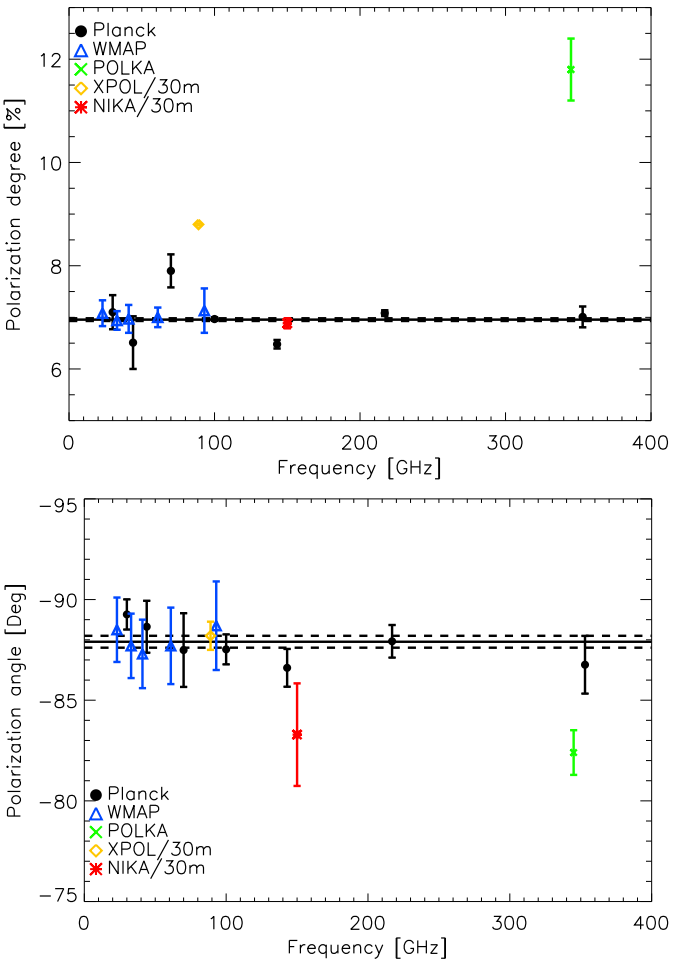

Fig. 6. *Top*: polarization degree as a function of frequency as measured by *Planck* (black dots), WMAP (blue triangles), XPOL (green diamond) and *NIKA* (red crosses). The *NIKA* value has been estimated by integrating in a radius of 5′ as given by XPOL (Aumont et al. 2010). The solid line represents the weighted-averaged degree of polarization accounting for low frequency values (<200 GHz) and excluding XPOL. Dashed lines are the uncertainties. *Bottom*: polarization angles in Galactic coordinates for the same five experiments given above. The solid line represents the weighted-averaged polarization angles.

4. Crab Spectral Energy Distribution in intensity and polarization

4.1. Intensity

The total intensity emission of the Crab nebula at radio and millimeter wavelengths (from 1 to 500 GHz) is mainly due to synchrotron emission and can be well described by a single power law of the form:

$$I_\nu = A(\nu/1\mathbf{GHz})^\beta \quad (4)$$

with spectral index β = -0.296±0.06 (Baars et al. 1977; Macías-Pérez et al. 2010). Further, the Crab nebula is fading with time at a rate of α = 0.167±0.015 % yr^{-1} (Aller & Reynolds 1985). These results suggest a low frequency emission produced by particles accelerated by the same magnetic field. Macías-Pérez et al. (2010) have shown also that there is no evidence for an extra synchrotron component and for a component of thermal dust emission at these frequencies. The direction of the polarization is therefore expected to be constant across the frequency range 30-300 GHz while the polarization degree may vary.

	I [Jy]	Q [Jy]	U [Jy]	I_{pol} [Jy]	p [%]	ψ [°]	$I_{pol} > 3\sigma_{I_{pol}}$
5′ FWHM centered	198.9±4.8	2.8±0.1	-16.1±0.2	16.3±0.3	8.2±0.1	140.0(-82.4)±0.2±0.5±1.8*	145.3(-87.6)±0.1±0.5±1.8*
7′ FWHM centered	226.4±5.7	3.2±0.2	-15.2±0.3	15.6±0.3	6.9±0.1	140.9(-83.3)±0.3±0.5±1.8*	145.2(-87.6)±0.1±0.5±1.8*

Table 2. *A systematic angle uncertainty of 1.8° must be considered in the polarization angle error budget. We also consider a 0.5° of uncertainty due to the intensity to polarization leakage correction. Total flux I, Q, and U, polarized intensity flux I_{pol}, polarization degree p, and angle ψ are here presented. The values have been calculated within 5′ and 7′ radius from the center of the map. The polarization angle has been also calculated where $I_{pol} > 3\sigma_{I_{pol}}$ to avoid the contribution of pixels biased by the noise. The polarization angle is here given in Equatorial coordinates and Galactic coordinates within parenthesis. A total calibration error of 10 % must be accounted for and propagated to the polarization estimates.

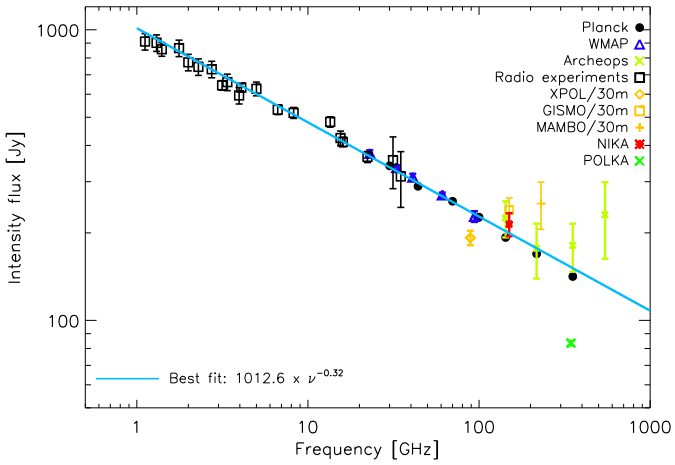

Fig. 7. Crab nebula total intensity SED as obtained from *Planck* (Planck Collaboration et al. 2016), *WMAP* (Weiland et al. 2011), Archeops (Macías-Pérez et al. 2007), radio experiments (Dmitrenko et al. 1970; Vinogradova et al. 1971), XPOL/30m (Aumont et al. 2010), *NIKA*30m (this paper), MAMBO/30m (Bandiera et al. 2002) and GISMO/30m (Arendt et al. 2011) data. The best-fit obtained by the analysis in this paper is shown in cyan line. Both, the best-fit models and the data account for the Crab nebula fading with the time.

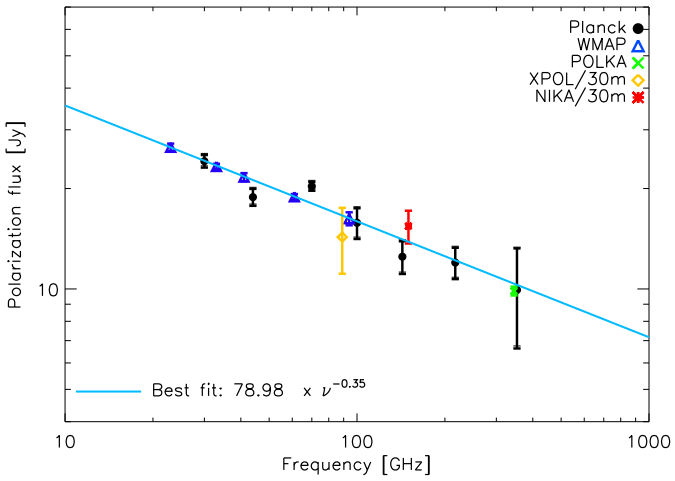

Fig. 8. Crab nebula polarization flux SED as obtained from the *Planck* (Planck Collaboration et al. 2016), *WMAP* (Weiland et al. 2011) and *NIKA* (this paper) data. The two best-fit models presented have been estimated using only WMAP data (blue line) or *Planck* data only (black line).

Fig. 7 shows the total intensity flux of the Crab nebula as a function of the frequency. The fluxes in the radio domain were taken from Dmitrenko et al. (1970) and Vinogradova et al. (1971). We also show microwave and mm wavelengths fluxes from *Archeops* (Macías-Pérez et al. 2007), *Planck* (Planck Collaboration et al. 2016), WMAP (Weiland et al. 2011), XPOL/30m (Aumont et al. 2010), MAMBO/30m (Bandiera et al. 2002) and GISMO/30m (Arendt et al. 2011). The HFI *Planck* data have been recomputed because of flux loss observed in previous results. These new results will be soon published by the *Planck* collaboration. The measured *NIKA* total intensity flux at 150 GHz is shown in red. Notice that in the plot both the best-fit model and the data represented are corrected for the fading of the source.

By χ^2-minimization we obtain the fit shown in cyan in Fig. 7. The best-fit parameters obtained are:

$$A = 1012.6 \pm 3.8; \qquad \beta = -0.324 \pm 0.001$$

The *NIKA* data are consistent with this model at 1σ level. The estimated spectral index β is slightly different from previous results provided by Macías-Pérez et al. (2010). This mainly concerns the addition of recently reviewed results of *Planck* (*in prep.*) and *WMAP* (*Weiland et al. 2011*).

As already discussed above XPOL/30m total power emission is low with respect to expectations. The POLKA value is found lower than Planck result at the same frequency, this is mainly explained by the spatial filtering of LABOCA data reduction as already discussed above.

4.2. Polarization

Though the total power emission of the Crab nebula has been monitored over decades across a large range of frequencies, the amount of polarization data is very small. Recent results provided by Planck (Planck Collaboration et al. 2016), WMAP (Weiland et al. 2011) and XPOL (Aumont et al. 2010) together with NIKA allow us to trace the spectral energy distribution of the polarized emission as shown in Fig. 8. Notice that the uncertainty for the NIKA value has been estimated propagating the absolute calibration error. Considering Eq. 4.1 as single power law like model for synchtron emission and accounting for fading the best-fit parameters A_{pol}, β_{pol} are:

$$A_{pol} = 78.98 \pm 7.82; \qquad \beta_{pol} = -0.35 \pm 0.03$$

XPOL and NIKA agree both power laws within 1σ error bar. In this case the XPOL data are not affected by the Stokes I map quality as in the case of the polarization degree measurement.

We have also estimated the spectral index of the Crab nebula polarization emission at high frequency using the map obtained by SCUPOL (Matthews et al. 2009) at 352 GHz (850 μm) and the NIKA map. Considering only the region observed by SCUPOL we obtain:

$$\beta_p = -0.33 \pm 0.01. \qquad (5)$$

This result is in good agreement with the best-fit model spectral index computed above.

5. Conclusions

The Crab nebula is considered as a celestial standard calibrator for CMB experiments in terms of polarization degree and angle. An absolute calibration is particularly important for the measurement of the CMB polarization B-modes, which are a window towards the physics of the early Universe.

We have reported in this paper first high angular resolution polarization observations of the Crab nebula at 150 GHz with the NIKA camera. These observations have allowed us to accurately map the spatial distribution of the polarization fraction and angle. Using all available polarization data to date we conclude that the polarization angle of the Crab nebula is consistent with being constant with frequency, from 23 GHz to 217 GHz, at arcmin scales with a value of -87.9° ±0.3 in Galactic coordinates. In addition, there is a strong case for a constant polarization degree consistent with a value of p = 6.95 ± 0.03%.

Moreover, we have characterized the intensity and polarization SED of the Crab nebula. In both total power and polarization, we find that the data are overall consistent with a single power law spectrum as expected from synchrotron emission. However, we find some discrepancies between data sets, which will require further mm measurements at high resolution for a better understanding of the physics at play. Among future polarization experiments, NIKA2 (Calvo et al. 2016), will provide high sensitive polarization observations of the Crab nebula adding a 260 GHz map at 11″ resolution.

References

Adam, R., Adane, A., Ade, P. A. R., et al. 2017, ArXiv e-prints arXiv:1707.00908
Adam, R., Comis, B., Macías-Pérez, J. F., et al. 2014, A&A, 569, A66
Aller, H. & Reynolds, S. 1985, The Astrophysical Journal, 293, L73
Arendt, R. G., George, J. V., Staguhn, J. G., et al. 2011, ApJ, 734, 54
Aumont, J., Conversi, L., Thum, C., et al. 2010, A&A, 514, A70
Baars, J., Genzel, R., Pauliny-Toth, I., & Witzel, A. 1977, Astronomy and Astrophysics, 61, 99
Bandiera, R., Neri, R., & Cesaroni, R. 2002, A&A, 386, 1044
Belloche, A., Schuller, F., Parise, B., et al. 2011, A&A, 527, A145
Calvo, M., Benoît, A., Catalano, A., et al. 2016, Journal of Low Temperature Physics, 184, 816
Catalano, A., Adam, R., Ade, P., et al. 2016, arXiv preprint arXiv:1605.08628
Catalano, A., Calvo, M., Ponthieu, N., et al. 2014, A&A, 569, A9
Dmitrenko, D., Tseitlin, N., Vinogradova, L., & Giterman, K. F. 1970, Radiophysics and Quantum Electronics, 13, 649
Ginzburg, V. L. & Syrovatskii, S. I. 1965, ARA&A, 3, 297
Gomez, H. L., Krause, O., Barlow, M. J., et al. 2012, ApJ, 760, 96
Hester, J. J. 2008, ARA&A, 46, 127
Kuz'min, A. D. & Udal'Tsov, V. A. 1959, Soviet Ast., 3, 39
Lobanov, A. P., Horns, D., & Muxlow, T. W. B. 2011, A&A, 533, A10
Macías-Pérez, J., Lagache, G., Maffei, B., et al. 2007, Astronomy & Astrophysics, 467, 1313
Macías-Pérez, J. F., Mayet, F., Aumont, J., & Désert, F.-X. 2010, ApJ, 711, 417
Matthews, B. C., McPhee, C. A., Fissel, L. M., & Curran, R. L. 2009, ApJS, 182, 143
Mayer, C. H., McCullough, T. P., & Sloanaker, R. M. 1957, ApJ, 126, 468
Michel, F. C., Scowen, P. A., Dufour, R. J., & Hester, J. J. 1991, ApJ, 368, 463
Monfardini, A., Adam, R., Adane, A., et al. 2014, Journal of Low Temperature Physics, 176, 787
Monfardini, A., Benoit, A., Bideaud, A., et al. 2011, ApJS, 194, 24
Monfardini, A., Swenson, L. J., Bideaud, A., et al. 2010, A&A, 521, A29
Montier, L., Plaszczynski, S., Levrier, F., et al. 2015, A&A, 574, A136
Moreno, R. 2010, Neptune and Uranus planetary brightness temperature tabulation, Tech. rep., ESA Herschel Science Center, available from ftp://ftp.sciops.esa.int/pub/hsc-calibration/PlanetaryModels/ESA2
Planck Collaboration, Ade, P. A. R., Aghanim, N., et al. 2016, A&A, 594, A26
Ritacco, A., Adam, R., Adane, A., et al. 2016, Journal of Low Temperature Physics, 184, 724
Ritacco, A., Ponthieu, N., Catalano, A., et al. 2017, A&A, 599, A34
Simmons, J. F. L., Aspin, C., & Brown, J. C. 1980, A&A, 91, 97
Simmons, J. F. L. & Stewart, B. G. 1985, A&A, 142, 100
Thum, C., Wiesemeyer, H., Paubert, G., Navarro, S., & Morris, D. 2008, PASP, 120, 777
Vinogradova, L. V., Dmitrenko, D. A., & Tsejtlin, N. M. 1971, Izvestiia Vysshaia Uchebn. Zaved., Radiofizika, 14, 157
Weiland, J. L., Odegard, N., Hill, R. S., et al. 2011, ApJS, 192, 19
Weiler, K. W. & Panagia, N. 1978, A&A, 70, 419
Weisskopf, M. C., Hester, J. J., Tennant, A. F., et al. 2000, ApJ, 536, L81
Wiesemeyer, H., Hezareh, T., Kreysa, E., et al. 2014, PASP, 126, 1027
Wiesemeyer, H., Thum, C., Morris, D., Aumont, J., & Rosset, C. 2011, A&A, 528, A11

Acknowledgements. We would like to thank the IRAM staff for their support during the NIKA campaigns. The NIKA dilution cryostat has been designed and built at the Institut Néel. In particular, we acknowledge the crucial contribution of the Cryogenics Group, and in particular Gregory Garde, Henri Rodenas, Jean Paul Leggeri, Philippe Camus. This work has been partially funded by the Foundation Nanoscience Grenoble, the LabEx FOCUS ANR-11-LABX-0013 and the ANR under the contracts "MKIDS", "NIKA" and ANR-15-CE31-0017. This work has benefited from the support of the European Research Council Advanced Grant ORISTARS under the European Union's Seventh Framework Programme (Grant Agreement no. 291294). We acknowledge fundings from the ENIGMASS French LabEx (R. A. and F. R.), the CNES post-doctoral fellowship program (R. A.), the CNES doctoral fellowship program (A. R.) and the FOCUS French LabEx doctoral fellowship program (A. R.).